Antiferromagnetic defect structure in LaNiO_{3−δ} single crystals

Bi-Xia Wang, S. Rosenkranz, X. Rui, Junjie Zhang, F. Ye, H. Zheng, R. F. Klie, J. F. Mitchell, and D. Phelan

Phys. Rev. Materials **2**, 064404 — Published 12 June 2018

DOI: 10.1103/PhysRevMaterials.2.064404

Antiferromagnetic defect structure in $LaNiO_{3-\delta}$ single crystals

B. Wang[1], S. Rosenkranz[1], X. Rui[2], J. Zhang[1,3], F. Ye[4], R.F. Klie[2], J. F. Mitchell[1,*], and D. Phelan[1,+]

[1]*Materials Science Division, Argonne National Laboratory, Argonne, Illinois 60439, USA*

[2]*Department of Physics, University of Illinois at Chicago, Chicago, Illinois 60607-7061, USA*

[3]*Materials Science and Technology Division, Oak Ridge National Laboratory, Oak Ridge, Tennessee 38731, USA*

[4]*Neutron Scattering Division, Oak Ridge National Laboratory, Oak Ridge, Tennessee 37831, USA*

Abstract:

The origins of the metal-insulator and magnetic transitions exhibited by perovskite rare-earth nickelates, $RNiO_3$, remain as open issues, with the roles of charge disproportionation, magnetic interactions, and lattice response across multiple length scales among the possibilities. Recently, growth of single crystals of $LaNiO_3$, which is the only member of these compounds that remains metallic in its ground-state, has been reported, opening a new chapter in the investigation of the perovskite nickelates. Here, using a combination of magnetometry, heat capacity, and neutron scattering on as-grown and purposely reduced $LaNiO_{3-\delta}$ crystals, we show that both antiferromagnetic and ferromagnetic phases with a Néel temperature of ~152 K and a Curie temperature of ~225 K can be induced by reduction of the oxygen content. Transmission electron microscopy shows that these phases are characterized by ordered oxygen vacancy defect structures that exist as dilute secondary phases in as-grown crystals despite growth in partial oxygen pressures up to at least 130 bar. The demonstration of antiferromagnetism resulting from oxygen vacancy ordered structures implies that stoichiometry must be explicitly considered

when interpreting bulk properties of $LaNiO_{3-\delta}$ single crystals; accordingly, the implications of our results for putative oxygen-stoichiometric $LaNiO_3$ are discussed.

I. Introduction

Rare-earth perovskite nickelates (RNiO$_3$) represent an important series that continues to challenge our understanding of how magnetic order and electrical transport behave in transition metal oxides and how they relate to the complex correlations of charges, spins, the lattice, and orbitals. Notably, aside from LaNiO$_3$, all compounds in the series undergo metal-insulator transitions (MIT) and possess insulating, antiferromagnetic (AFM) ground-states [1]. These transitions have been shown to correlate with the e_g bandwidth, which is modulated by the R^{3+} ionic radii via Ni-O-Ni bonds angles [2]. A structural phase transition (*Pnma* to $P2_1/n$) occurs simultaneously with the MIT for R≠La [3], and this MIT has been discussed in terms of charge disproportionation, Jahn-Teller distortions, charge-transfer, covalency, and ligand holes [4–19]. In particular, one interpretation of the MIT is that it arises due to the disproportionation of charge on nickel sites, such that charge order occurs which breaks the *Pnma* symmetry in the low temperature, insulating phase [3,4,16]. Recently, an alternative scenario which is commonly referred to as bond disproportionation, has received significant attention [6–8,19]. In this mechanism, ligand holes play an important role such that the transfer of charge between oxygen anions and nickel cations leads to the disproportionation and concomitant inequivalent magnetic moments on charge sublattices [19]. Bond disproportionation has been used to interpret recent x-ray absorption and resonant inelastic x-ray scattering spectroscopies [8] and has been favored in recent double-cluster calculations [19]. Nevertheless, the mechanism of the MIT continues to be a focus of both experimental and theoretical work in nickelates.

For small bandwidth nickelates (R^{3+} radius < Nd^{3+}), the MIT occurs at a higher temperature than the AFM transition, demonstrating that charge and spin are the primary and secondary order parameters, respectively [15–17]. However, the simultaneous occurrence of AFM and MIT for R = Nd/Pr, opens the question as to whether there is a cross-over in the primary and secondary order parameters upon increasing bandwidth [13,17–19]. In this context, it is interesting to consider $LaNiO_3$, which has behavior that has long been understood to deviate from the remainder of the series. In particular, $LaNiO_3$ has been described as Pauli paramagnetic [1,2,16], metallic [23–25], and rhombohedral [24,26] spanning from low (~ 4 K) to at least room temperature. Neither MIT [23–25] nor long-range structural phase transition [26] has been reported, and powder neutron diffraction measurements have to date revealed no evidence of antiferromagnetic ordering [26]. Yet, clearly this compound lies extremely close to magnetic and structural transitions, and recently experimental and theoretical considerations have cast doubt upon whether the simple picture of a rhombohedral, paramagnetic metallic ground-state is appropriate. For example, two recent reports of pair density function analysis of neutron diffraction data [12,13] favor a monoclinic description of the local environment in $LaNiO_3$ to at least 200 K. This would imply charge disproportionation akin to the long-range charge ordered structure that occurs for all other $RNiO_3$ [16,27,28]at least on local length scales. First principles calculations indicate that rhombohedral and orthorhombic structures lie very close in energy – indeed, so close that fluctuations between these structures may occur [11]. Breathing modes and antiferromagnetic ordering were both found to be energetically favorable (breathing modes significantly more-so) [11].

Whereas the bulk of all previous work has been performed on polycrystalline materials, advances in high pressure floating-zone growth have recently led to two reports of single crystal

growth of $LaNiO_{3-\delta}$, but differing interpretations have led to uncertainty regarding its intrinsic behavior. Zhang *et al*. reported single crystals possessing rhombohedral symmetry, metallic behavior, and no obvious magnetic ordering based on both magnetic susceptibility and heat capacity, although a broad maximum in the susceptibility was observed at ~ 200 K [29]. On the other hand, Guo *et al*. have reported metallic, rhombohedral single crystals with anomalies in both the heat capacity and magnetic susceptibility occurring at T_N ~ 157 K [14]. Consistent with these results, they reported the appearance of magnetic Bragg reflections via single-crystal neutron diffraction below T_N. If Guo *et al.*'s results are borne out, they would lead to a radical and different interpretation of the physics of $LaNiO_3$, which would revise not only our understanding of bulk $LaNiO_3$, but also of thin films [30–33], and heterostructures [25–26].

$LaNiO_3$ may be proximal to an intrinsic quantum critical point [11], so it is especially important to recognize that stoichiometry and defects can also lead to dramatic modifications of the physical properties [37]. Indeed, although single crystals provide meaningful direction-dependent information that cannot be obtained from polycrystalline specimens and are favored for electrical transport studies, the control of stoichiometry and in some cases defects and impurities can, in fact, present a more significant challenge in large oxide crystals than in bulk polycrystalline materials. Both ferromagnetic and AFM oxygen-deficient phases have previously been reported in polycrystalline lanthanum nickelates [37,38] with T_N close to that reported for the $LaNiO_3$ single crystals by Guo *et al* [14]. This led us to explore the effects of oxygen defects in $LaNiO_{3-\delta}$ single crystals. Here, using a combination of magnetometry, heat capacity, and neutron scattering, we report stabilization of not only an AFM minority phase, $LaNiO_{2.5}$, with T_N ~ 152 K, but also a ferromagnetic phase, $LaNiO_{2.75}$ with T_C ~225 K, both of which we have intentionally induced in $LaNiO_{3-\delta}$ via systematic reduction of the oxygen content.

The ordering of oxygen vacancies in these minority phases are further demonstrated by Transmission Electron Microscopy (TEM) measurements.

II. Experimental Details

Single crystals of $LaNiO_{3-\delta}$ were grown using a high-pO_2 floating zone furnace (HKZ-1; SciDre GmbH) under 40 bar and 130 bar pO_2 as described in Ref. [29]. As reported previously [4], the oxygen content of a specimen taken from the $LaNiO_{3-\delta}$ single crystals grown under 40 bar pO_2 was determined to be 2.985(3), i.e., $\delta \approx 0.015(3)$ vacancies/formula unit using thermogravimetric analysis (TGA) measurements. We have obtained similar values ($\delta \approx 0.020(2)$) from TGA study for a specimen taken from a growth under 130 bar pO_2. Thus, all of our as-grown crystals possess a finite, but small quantity of oxygen deficiency prior to any of our measurements, despite high oxygen pressure growth. Specimens for structural and bulk properties characterization were prepared by extracting from boules of as-grown single crystals. Specifically, for heat capacity and magnetization measurements a 22.2 mg specimen was extracted from the crystal boule grown under 40 bar pO_2, and neutron scattering was carried out on samples (~1 g) from single crystals grown under both 40 bar and 130 bar pO_2. Heat capacity measurements were performed in a Quantum Design Physical Property Measurement System (PPMS) in the temperature range of 130-190 K. Apiezon-N vacuum grease was employed to fix the crystal to the sapphire sample platform, and addenda measurements were subtracted. DC magnetic susceptibility measurements were performed in a Quantum Design Magnetic Property Measurement System (MPMS-3). Field-cooled and zero-field cooled temperature-dependent susceptibility data were collected under an external field of $\mu_0 H = 5.0$ T. Neutron diffraction

experiments were performed on CORELLI [39], a time-of-flight diffractometer at the Spallation Neutron Source (SNS) located at Oak Ridge National Laboratory (ORNL) that employs a pseudo-white neutron beam and uses cross-correlation to extract the elastic signal. Because of the twinning of the crystals, we employ a pseudocubic notation when indexing peaks with the aristotype perovskite cell that contains one formula unit (a~3.9 Å). By design, CORELLI provides an extremely broad wave-vector coverage with a large signal-to-noise. To further enhance the visibility of weak peaks, data measured in different octants of reciprocal space were symmetrized using Laue class *mmm*. The scattering from both the 40 bar and 130 bar crystals was dominated by a single, large, twinned crystal in each case, and some impurity peaks, three to four orders of magnitude weaker than the dominant crystal's Bragg peaks, were observed. These weak impurity peaks could be easily discriminated from peaks that are intrinsic to the $LaNiO_{3-\delta}$ crystal by whether or not they are commensurate with the dominant structure.

Magnetometry, heat capacity, and neutron scattering experiments were performed on as-grown and oxygen reduced single crystals in order to directly explore the effects of intentionally-induced oxygen deficiency. *Crucial to the design of the experiment, the exact same specimens were measured before and after reduction*. Reduction was conducted on a TGA balance (Mettler-Toledo model DSC 1) in a 4% H_2/N_2 gas mixture. The sample was annealed at temperature intervals of 25 °C from 250 °C up to 400 °C, holding at 24 hours for each temperature. The total weight loss (~ 88 μg) of the 22.2 mg crystal (grown under pO_2 40 bar), which was used for both the magnetometry and heat capacity measurements, provides an estimate of the average stoichiometry of $LaNiO_{2.924(3)}$ post-reduction, assuming a starting stoichiometry of $\delta = 0.015(3)$ [4]. The weight loss (~4.4 mg) of the ~1.14 g crystal grown under 130 bar used for the neutron scattering measurements gives an average stoichiometry of

$LaNiO_{2.921(2)}$ post-reduction, assuming a starting stoichiometry of $\delta = 0.020(2)$. We emphasize that these stoichiometry values represent an average from a single region of the grown boules and that a nonuniform oxygen content variation is likely given the floating zone growth. Furthermore, as we discuss below, the reduction of the single crystal almost certainly leads to an inhomogeneous, core-shell type of structure with the shell likely having significantly more oxygen vacancies than the core.

TEM, including high-resolution phase contrast imaging, electron diffraction and scanning transmission electron microscopy (STEM) imaging was performed on another as-grown single crystal (pO_2 = 40 bar). Selected area electron diffraction pattern (SAED) and phase-contrast TEM imaging was used to analyze the direction and periodicity of putative oxygen vacancy ordering, while scanning transmission electron microscope (STEM) images were used to directly visualize the oxygen vacancy ordering in $LaNiO_{3-\delta}$ at the atomic-scale. The SAED and TEM images were acquired using a JEOL JEM3010 operated at 300 keV. Low-angle annular dark-field (LAADF) and annular bright-field (ABF) images were acquired using a probe aberration-corrected JEOL JEM-ARM 200CF equipped with cold field emission gun. The convergence semi-angle for STEM images was 13.4 mrad, and the collection semi-angles for LAADF and ABF detectors were set at range of 40-160 mrad and 11-25 mrad, respectively. The $LaNiO_{3-\delta}$ TEM samples were prepared by crushing single crystal $LaNiO_{3-\delta}$ using mortar and pestle following by an ultrasonic treatment in isopropanol and drop-casting on a holey carbon TEM grid. To avoid beam induced artifacts, the samples were not exposed to any Ar^+ beam thinning.

III. Results and Discussion

We begin by considering the nature of the oxygen vacancies present in our as-grown sample that had been prepared under 40 bar pO_2, which characterization via TGA on a specimen removed from a growth under the same pressure yielded $\delta \sim 0.015(3)$, though we generally expect that there exists variation between specimens due to oxygen inhomogeneities present during floating zone growth. TEM imaging and electron diffraction (Fig. 1) reveal oxygen vacancy ordering in a small concentration of regions. Fig. 1(a) shows a low magnification image of a $LaNiO_{3-\delta}$ particle, which contains areas of $LaNiO_3$ for which no oxygen vacancy ordering is detected as well as oxygen vacancy ordered $LaNiO_{3-\delta}$. Fig. 1(b) shows an electron diffraction pattern from the region of $LaNiO_3$ for which no vacancy ordering was detected in the (0, 1, 1) orientation. As expected for a crystal in the rhombohedral space group *R-3c*, the only reflections that are observed that break cubic symmetry occur at the *R*-points of the cubic Brillouin zone (½ ½ ½). We note that in principle not all *R*-points are systematically allowed for *R-3c*, but the presence of multiple scattering (i.e., Renninger effects) in diffraction experiments is well known to cause violations of the systematic absences and we consider that to be likely here based on our experience with single crystal diffraction on other rhombohedral perovskites. Fig. 1(c) shows an electron diffraction pattern for oxygen vacancy ordered regions $LaNiO_{3-\delta}$, where superlattice reflections are visible at ($^1/_2$, $-^1/_4$, $^1/_4$), ($^1/_2$, $-^3/_4$, $^3/_4$), ($^1/_2$, 0, 0), known as *X*-points, and (0, $^1/_2$, $^1/_2$) known as *M*-points. The ($^1/_2$, $-^1/_4$, $^1/_4$) and ($^1/_2$, $-^3/_4$, $^3/_4$) superlattice reflections have been previously reported for $LaNiO_{2.75}$ by Gonzalez-Calbet et al. [40]. Atomic-resolution STEM imaging (Fig. 1(d)) shows an area of oxygen vacancy ordering in $LaNiO_{2.75}$ as well as an area where no oxygen vacancy ordering was detected.

It is interesting to note here that we also found areas (Supplementary Fig. 1(a) [41]) where the oxygen vacancies appear to order along the (0, -1, 1) direction, which has been

previously reported for $LaNiO_{2.5}$ [37,42–46]. The electron diffraction pattern from this area is shown in Supplementary Fig. 1(b) [41] while the corresponding atomic-resolution STEM image is shown in Supplementary Fig. 1(c) [41]. In this ABF image, the La, Ni and O atomic columns are clearly visible, and it can be seen that the oxygen atomic columns show a periodic displacement in every second unit cell along the (0, -1, 1) direction. The vacancy ordering proposed for $LaNiO_{2.5}$ [37,44,46] is shown in Supplementary Fig. 2 [41], though we note that there consensus lacking in the literature regarding the proper space group [3,37,40,42,45,47] The corresponding SAED pattern shows superlattice reflections at *X* and *M* points in agreement with the vacancy-ordered structural motif.

Our TEM analysis shows that two oxygen deficiency structures, $LaNiO_{2.75}$ and $LaNiO_{2.5}$, were present in the as-grown (pO_2 = 40 bar) $LaNiO_{3-\delta}$ sample and that the distribution of ordered oxygen vacancies form small regions of these defect phases. We emphasize here that the electron diffraction pattern for the region identified as $LaNiO_{2.75}$ shows additional superlattice spots at *X* and *M* points (see Fig. 1(c)). These reflections were not reported by Gonzalez-Calbet et al. [40], but they match with the superlattice spots for $LaNiO_{2.5}$. Diffraction patterns from a different region of the same sample are shown in Supplementary Fig. 3 [41], where only superlattice reflections consistent with the presence of $LaNiO_{2.75}$ are visible. We therefore believe that the diffraction pattern from the area shown in Fig. 1(c) arises due to the presence of a mixture of both $LaNiO_{2.75}$ and $LaNiO_{2.5}$.

We now consider the magnetic susceptibility (χ) and heat capacity (C_p) of an as-grown ~ 22.2 mg crystal (grown under pO_2 ~ 40 bar), which are shown in Fig. 2(a) and 2(b). A broad maximum centered at T ~ 200 K, which is consistent with previous reports of as-grown crystals by Guo *et al.* [14] and Zhang *et al.* [29], was observed in χ. The origin of this broad feature is an

open question, as is whether or not it is intrinsic to stoichiometric $LaNiO_3$. It is notable that earlier work on polycrystals evidenced markedly different temperature dependences [5]. Heat capacity is featureless in the temperature range between 130 and 190 K. Thus, neither C_p or χ indicates any evidence of structural or magnetic transitions for the as-grown crystal over this temperature range.

Fig. 2(c) and 2(d) show identical measurements performed on the same 22.2 mg crystal specimen after reduction. It is immediately apparent that significant changes were induced by the reduction. In contrast to the as-grown crystal, χ rises below T~225 K on cooling, reaches a plateau between 225 K and 152 K, and then decreases below 152 K. Furthermore, a broad peak in C_p/T, which was not apparent in the as-grown crystal, is observed at ~152 K. The increase in susceptibility at T_C ~ 225 K suggests a ferromagnetic ordering, while the decrease below T_N ~ 152 K implies antiferromagnetic ordering. We note that the oxygen vacancy-ordered phase $LaNiO_{2.75}$ has been reported to be ferromagnetic with T_C ~ 230 K [42], which implicates this impurity gives as the source of the ferromagnetic ordering observed in our $LaNiO_{3-\delta}$ specimen. Similarly, $LaNiO_{2.5}$ [34,37–40] has been reported to be antiferromagnetic with T_N~140 K. The proximity of this reported T_N to that observed in our oxygen deficient crystal suggests that this impurity may be responsible for the apparent antiferromagnetic transition. These bulk measurements therefore point to a scenario in which the reduction process increases the concentration of regions of ordered oxygen vacancies possessing the $LaNiO_{2.5}$ and $LaNiO_{2.75}$ phases, which are present in dilute amounts in as-grown crystals. However, the nature of the reduction process likely leads to an inhomogeneous, core-shell like structure in which the shell has a significantly higher oxygen vacancy concentration than the core. Although the line phases, $LaNiO_{2.5}$ and $LaNiO_{2.75}$, represent perfectly ordered lanthanum nickelate defect structures, there

are certainly intermediate compositions that possess values of δ that are not precisely 0.5 and 0.25. As an example, Moriga *et al*. compared the magnetic properties of $LaNiO_{2.51}$ and $LaNiO_{2.54}$, and it appeared that the latter sample possessed a higher T_N. It is logical to suspect that oxygen deficient regions with varying values of δ are present after reduction, and this likely leads to variance in T_N which contributes to the broadness of the peak that we observed in C_p observed around 152 K after reduction.

Given the changes in magnetic behavior induced by reduction, we used single crystal neutron diffraction to further explore the magnetic ordering. Here, we focus on scattering from the single crystal grown under pO_2 of 130 bar (1.14 g); results from the single crystal grown under 40 bar are discussed further below. Fig. 3(a) and 3(b) compare the pseudocubic $(h,k,{}^1/_4)$ scattering plane of the 130 bar crystal before and after reduction. We note that the crystal was measured in the same sample environment for both measurements, and we have used nuclear Bragg reflections to normalize the intensities, allowing for direct comparison. Weak, temperature-dependent Bragg peaks indexed with a wave-vector of $\boldsymbol{q_m} = ({}^1/_4, {}^1/_4, {}^1/_4)$ in pseudocubic notation are observed after reduction, but were not observable in the as-grown crystal. The temperature dependence of these peaks (Fig. 4(a) and 4(c)) evidences that they appear below approximately the same T_N observed in both susceptibility and heat capacity, thereby confirming their antiferromagnetic nature. The intensity of these peaks is enhanced by intentional reduction because the concentration of the oxygen vacancy-ordered regions is increased. That the density of the antiferromagnetic defect structure regions increases after reduction in small pieces (pO_2=40 bar) as well as large (pO_2=130 bar) pieces implies a consistency in the transformation across processing conditions (regardless of size or initial growth pressure).

In addition to the temperature-dependent magnetic Bragg reflections discussed above, the reduction also induces structural modulations. From Fig. 3(a) and 3(b), it is apparent that peaks indexed with a wave-vector of $\boldsymbol{q_s} = (^1/_2, ^1/_4, ^1/_4)$ are also present after reduction, but are below our detection limit in the measurement performed before reduction. These peaks are observed up to large values of $|\boldsymbol{Q}| = 10$ Å^{-1}, suggesting that they are not of magnetic origin but rather arise from a structural modulation. Moreover, as shown in Fig. 4(b) and 4(d), these peaks are temperature-independent up to at least 200 K. Finally, we note that these peaks possess the same wave-vector observed in the oxygen-vacancy ordered regions by TEM, which confirms that they are structural and arise due to oxygen vacancy ordering. The observed magnetic wave-vector indicates that the magnetic unit cell is doubled along one pseudocubic axis with respect to this vacancy-ordered structure.

Other changes induced by reduction are observed at the pseudocubic Brillouin zone boundaries. Consider first the as-grown sample with a small concentration of defect regions, as shown in the intensity map of the $l = ^1/_2$ plane in Fig. 5(a), we observed strong peaks at the *R* points and extremely weak peaks at *X* and *M* points. This evinces a dilute concentration of the oxygen-ordered phases which yield reflections at *X* and *M* in the as-grown sample, consistent with the TEM results described above. The reason that these are visible when the magnetic peaks are not is because their structure factors are intrinsically much larger than those of the magnetic peaks. Because of the dilute but finite concentration of ordered defect phases, it is impossible to use the observed scattering at the *X* and *M* points to support the claim that the rhombohedral (space group *R-3c*) symmetry is broken in stoichiometric $LaNiO_3$. [48] Nevertheless, upon reduction, the scattering at the *X* and *M* points significantly increases, as shown in Fig. 5(b), consistent with an increasing phase fraction of the vacancy-ordered phases.

Our neutron data provides no evidence of symmetry breaking of stoichiometric $LaNiO_3$, and given that the electron diffraction data in regions where ordered vacancies are not present (Fig. 1(b)) evidences only pseudocubic Brillouin zone boundary peaks at *R* and not *X* or *M* points, it is reasonable to conclude that average structure of the ground-state of stoichiometric $LaNiO_3$ is rhombohedral.

IV. Summary and Conclusions

We summarize our findings as follows. The crystals that we have synthesized at pressures of 40 bar and 130 bar pO_2 tend to grow nearly stoichiometric, but there is a finite, non-zero concentration of oxygen vacancies (~0.02) present found in specimens taken from as-grown boules in both cases. Microscopy clearly establishes that there is a tendency of these vacancies to form ordered defect regions, which appear to have $LaNiO_{2.5}$ and $LaNiO_{2.75}$ structures, and are antiferromagnetic and ferromagnetic [37], respectively. Depending on their relative concentrations, these defect regions can easily lead to difficulties in interpreting the intrinsic properties of stoichiometric $LaNiO_3$ based on single crystal specimen. Because the concentrations may depend upon both the radial position (i.e., core or surface of the rod) as well as the position along the growth axis, it is important to realize that stoichiometry or lack of detectable impurities within a small piece removed from a rod may not reflect the overall composition of larger samples used for neutron scattering studies.

An example of the confusion in interpreting the results of a neutron scattering experiment is given in Fig. 6, which shows the neutron scattering pattern measured from another as-grown crystal (grown at pO_2 40 bar). In contrast to the measurements shown in Fig. 3(a), which had been performed on an as-grown crystal at pO_2 of 130 bar, we observed magnetic peaks at $\boldsymbol{q_m}$ =

($^1/_4$,$^1/_4$,$^1/_4$) from this particular crystal without reduction, even though TGA analysis performed on small pieces of boules grown under 130 bar and 40 bar yielded similar oxygen contents for as-grown crystals. Given that such peaks were only observed in the 130 bar crystal after intentional reduction, we conclude that the magnetic ordering wavevector was observable in the as-grown (pO_2 = 40 bar) crystal because this particular specimen has a larger concentration of the $LaNiO_{2.5}$ phase.

Concerning stoichiometric, bulk $LaNiO_3$, our present measurements evidence nothing that contradicts the picture of a non-magnetically-ordered, metallic ground-state. Nor do they confirm that this is the ground-state because of the defects that are inherently present in our specimens. Instead, our results do confirm that AFM ordering is induced concomitant with ordered oxygen defect structures upon hydrogen reduction of $LaNiO_{3-\delta}$. There are two possibilities for reconciling the results of Guo *et al.* [14] with the present work. The first is that, as argued by Guo *et al.*, the antiferromagnetic ground-state that they observed is an intrinsic property of $LaNiO_3$ that requires extremely pure samples that are stoichiometric (Guo *et al.* reported δ=0.002 as derived from the initial and final masses measured in TGA [14]). The second is that the neutron-sized samples measured by Guo *et al.* may possess oxygen-ordered regions that were not observed in the TGA measurement which would have been performed on a much smaller specimen, in which case the antiferromagnetism would result from these regions. Ultimately, the present work cannot definitively distinguish between these two possibilities.

However, the present work does offer a mechanism by which these two possibilities could be resolved and by which future studies should be judged. We suggest that when future neutron scattering measurements are reported on single crystal $LaNiO_3$, measurements over reciprocal space regions that contain M, X, and (¼, ¼, ½) propagation vectors from the cubic Γ

point should also be reported, since the present work shows that these are clearly nuclear peaks that are correlated with oxygen-deficient regions. If these points are absent in a sample that possesses an antiferromagnetic Bragg peak, then that would argue that the antiferromagnetism is an intrinsic property of stoichiometric $LaNiO_3$; otherwise, the antiferromagnetism would originate from oxygen vacancy ordering.

Although we presently do not understand the broad maximum in the susceptibility at 200 K, the decrease in susceptibility upon cooling may perhaps be interpreted as evidence for fluctuating antiferromagnetic correlations. If true, this behavior would represent a deviation from the conventional view of the system as being a Pauli paramagnet. However, as we asserted in Ref. [29], we cannot rule out the possibility that the small oxygen deficiency is behind this maximum, though measurements on polycrystals of $LaNiO_{2.5}$ and $LaNiO_{2.75}$ do not exhibit it [37,42]. Overall, our results highlight that stoichiometry should be carefully considered when interpreting the intrinsic physical properties of the rare earth nickelates, particularly as new compositions continue to emerge with developing high pressure floating-zone technology. The suggested bond disproportionation mechanism of the MIT in nickelates suggests that the transfer of charge between Ni cations and oxygen anions plays a pivotal role in the bulk electronic and magnetic properties of nickelates; as such, the presence of oxygen vacancies in nickelate samples is an important consideration. Finally, our results clearly demonstrate that topotactic reduction of perovskite nickelate single crystals is a viable means for investigating ordered oxygen vacancies and exploring the physics of these reduced phases.

Acknowledgements

Work in the Materials Science Division at Argonne National Laboratory was supported by the U.S. Department of Energy, Office of Science, Basic Energy Sciences, Materials Science and Engineering Division. This research has been supported in part by ORNL Post Doctorial Development Fund by UT-Battelle, LLC under Contract No. DE-AC05-00OR22725 with the U.S. Department of Energy. Research at Oak Ridge National Laboratory was sponsored by the Scientific User Facilities Division, Office of Basic Energy Sciences, U.S. Department of Energy. The acquisition of JEOL JEM ARM200CF at the University of Illinois at Chicago (UIC) was supported by an MRI-R2 grant from the National Science Foundation(Grant No. DMR-0959470). The use of instrumentation at UIC Research Resources Center (RRC-East) is acknowledged.

Figure Captions:

Fig. 1: (a) Low magnification TEM image of an as-grown $LaNiO_{3-\delta}$ sample ($\delta \sim 0.015$). (b) Selected area electron diffraction (SAED) pattern of $LaNiO_3$ for which no oxygen vacancy ordering was detected from area shown in (a). (c) SAED pattern in the pseudocubic (0,1,1) orientation from different region shown in (a). Superlattice reflections corresponding to the oxygen vacancy ordering are indexed. (d) Atomic-resolution STEM-LAADF image of $LaNiO_{3-\delta}$ showing a domain of oxygen vacancy ordered $LaNiO_{2.75}$ and one where no vacancy ordering could be detected. The FFT of the oxygen vacancy ordered domain is shown an insert. All measurements were performed at room temperature.

Fig. 2: Temperature dependence of the heat capacity and magnetic susceptibility of as-grown (a,b) (δ ~ 0.015) and reduced (c,d) (δ ~ 0.076) $LaNiO_{3-\delta}$ single crystal (pO_2 = 40 bar).

Fig. 3: Elastic neutron scattering intensity of the (h,k,$^1/_4$) scattering plane at 6 K for as-grown (a) (δ ~ 0.020) and reduced (b) (δ ~ 0.079) $LaNiO_{3-\delta}$ single crystal (pO_2 = 130 bar).

Fig. 4: Temperature dependence of the neutron intensity measured after reduction for (a, c) the ($^1/_4$, $^1/_4$, $^1/_4$) peak and (b,d) the ($^1/_2$,$^5/_4$,$^1/_4$) peak (pO_2 = 130 bar, δ ~ 0.079).

Fig. 5: Elastic neutron scattering intensity of the (h,k,$^1/_2$) scattering plane at 6 K for as-grown (a) (δ ~ 0.020) and reduced (b) (δ ~ 0.079) $LaNiO_{3-\delta}$ single crystals (pO_2 = 130 bar).

Fig. 6: Elastic neutron scattering intensity of (h,k,$^1/_4$) scattering plane at 6 K for an as-grown $LaNiO_{3-\delta}$ single crystal that had been grown under pO_2 40 bar (δ~0.015).

Fig. 1

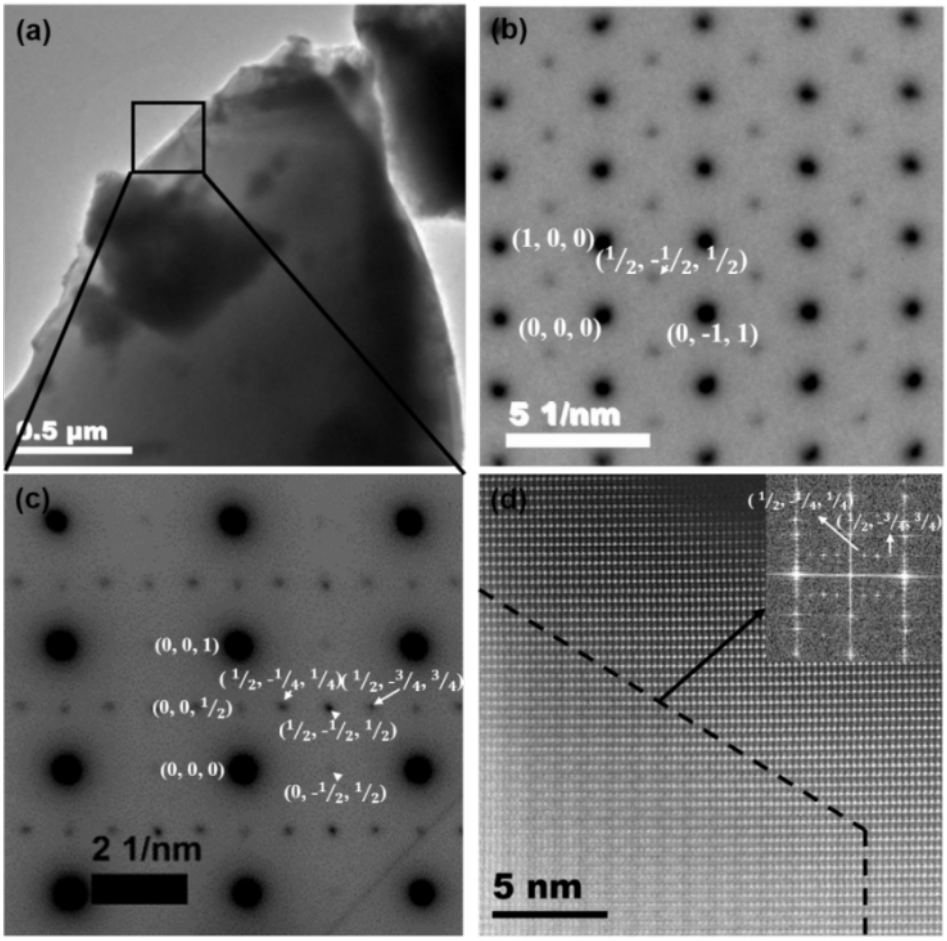
(a)
0.5 μm
(b)
(1, 0, 0)
(1/2, -1/2, 1/2)
(0, 0, 0)
(0, -1, 1)
5 1/nm
(c)
(0, 0, 1)
(1/2, -1/4, 1/4)
(1/2, -3/4, 3/4)
(0, 0, 1/2)
(1/2, -1/2, 1/2)
(0, 0, 0)
(0, -1/2, 1/2)
2 1/nm
(d)
(1/2, 3/4, 1/4)
(1/2, -3/4, 3/4)
5 nm

Fig. 2

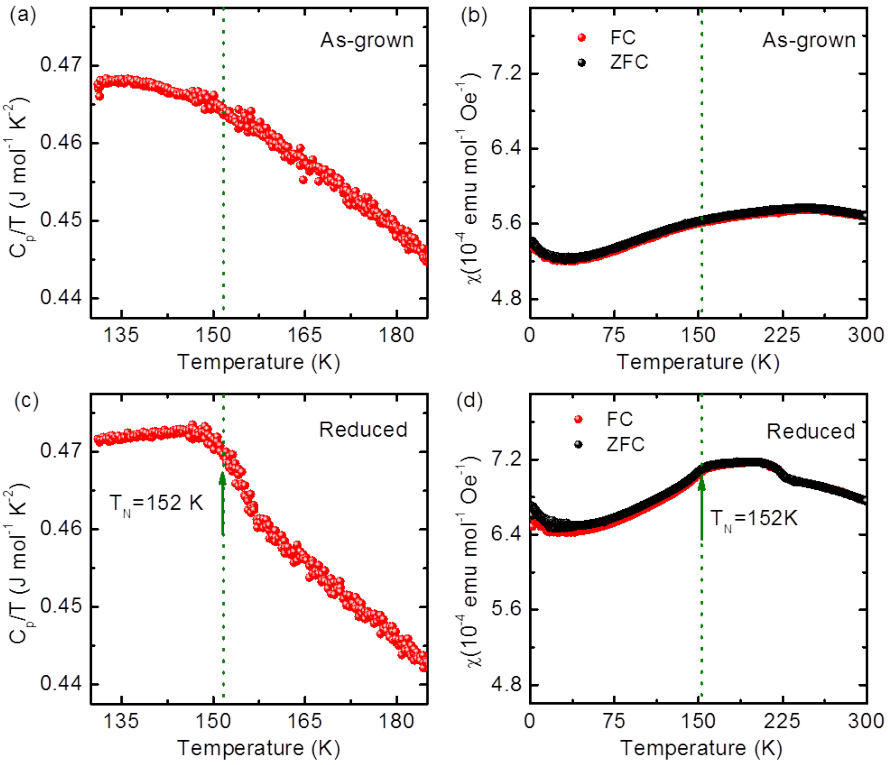
(a)
As-grown
0.47
0.46
0.45
0.44
C_p/T (J mol^{-1} K^{-2})
135
150
165
180
Temperature (K)
(b)
FC
ZFC
As-grown
7.2
6.4
5.6
4.8
χ(10^{-4} emu mol^{-1} Oe^{-1})
0
75
150
225
300
Temperature (K)
(c)
Reduced
T_N=152 K
0.47
0.46
0.45
0.44
C_p/T (J mol^{-1} K^{-2})
135
150
165
180
Temperature (K)
(d)
FC
ZFC
Reduced
T_N=152K
7.2
6.4
5.6
4.8
χ(10^{-4} emu mol^{-1} Oe^{-1})
0
75
150
225
300
Temperature (K)

Fig. 3

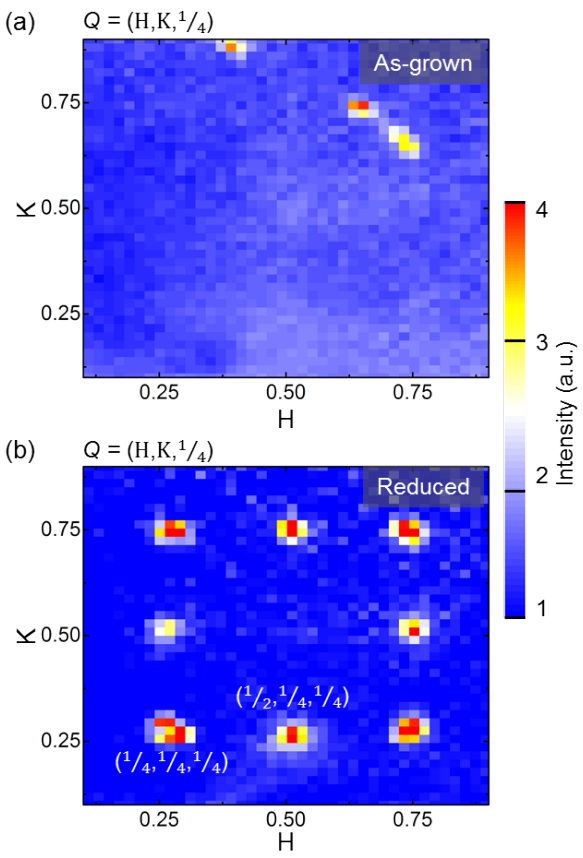
(a)
Q = (H,K,1/4)
As-grown
0.75
0.50
0.25
K
0.25
0.50
0.75
H
(b)
Q = (H,K,1/4)
Reduced
0.75
0.50
0.25
K
(1/2,1/4,1/4)
(1/4,1/4,1/4)
0.25
0.50
0.75
H
4
3
2
1
Intensity (a.u.)

Fig. 4

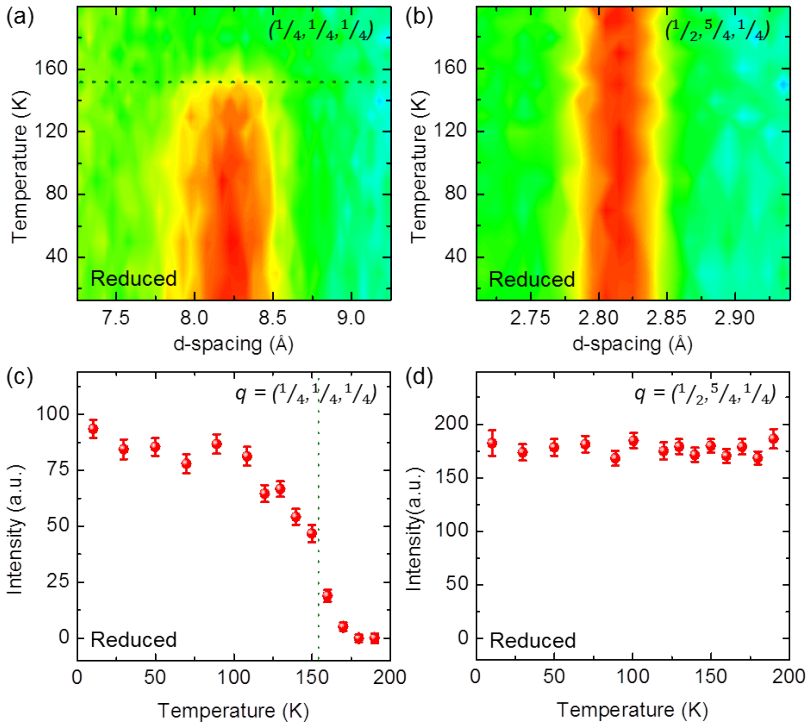
(a)
(1/4, 1/4, 1/4)
Temperature (K)
160
120
80
40
Reduced
7.5
8.0
8.5
9.0
d-spacing (Å)
(b)
(1/2, 5/4, 1/4)
Temperature (K)
160
120
80
40
Reduced
2.75
2.80
2.85
2.90
d-spacing (Å)
(c)
q = (1/4, 1/4, 1/4)
Intensity (a.u.)
100
75
50
25
0
Reduced
0
50
100
150
200
Temperature (K)
(d)
q = (1/2, 5/4, 1/4)
Intensity(a.u.)
200
150
100
50
0
Reduced
0
50
100
150
200
Temperature (K)

Fig. 5

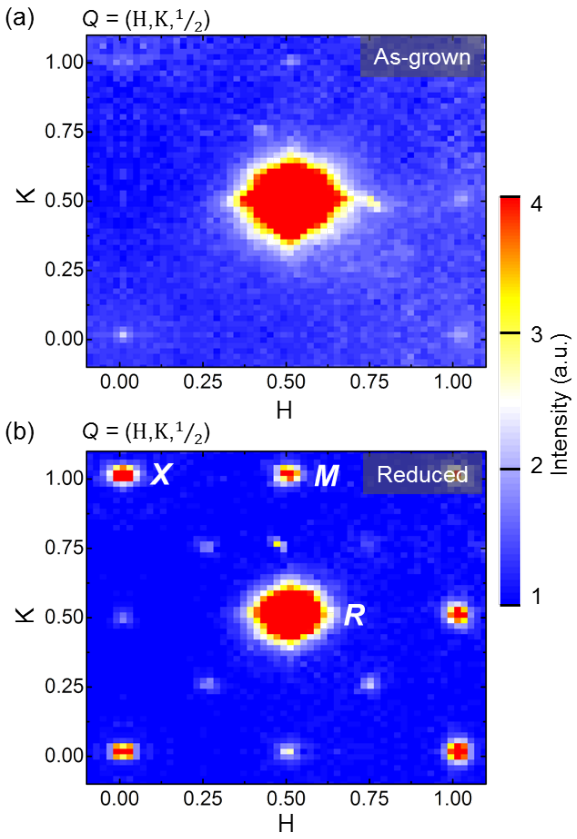
(a)
Q = (H,K,1/2)
As-grown
1.00
0.75
0.50
0.25
0.00
K
0.00
0.25
0.50
0.75
1.00
H
(b)
Q = (H,K,1/2)
X
M
Reduced
R
4
3
2
1
Intensity (a.u.)

Fig. 6

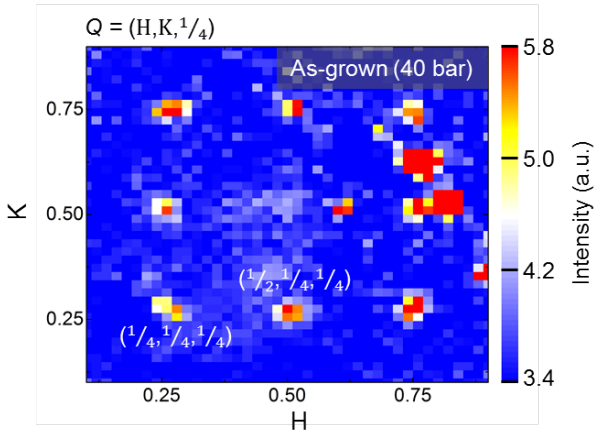
Q = (H,K,1/4)
As-grown (40 bar)
0.75
0.50
0.25
K
0.25
0.50
0.75
H
(1/2, 1/4, 1/4)
(1/4, 1/4, 1/4)
5.8
5.0
4.2
3.4
Intensity (a.u.)

*Email: mitchell@anl.gov; +Email: dphelan@anl.gov

References

[1] J. B. Torrance, P. Lacorre, A. I. Nazzal, E. J. Ansaldo, and C. Niedermayer, Phys. Rev. B **45**, 8209 (1992).

[2] J. L. García-Muñoz, J. Rodríguez-Carvajal, P. Lacorre, and J. B. Torrance, Phys. Rev. B **46**, 4414 (1992).

[3] J. A. Alonso and J. L. García-Muñoz, Phys. Rev. Lett. **82**, 3871 (1999).

[4] I. I. Mazin, D. I. Khomskii, R. Lengsdorf, J. A. Alonso, W. G. Marshall, R. M. Ibberson, A. Podlesnyak, M. J. Martínez-Lope, and M. M. Abd-Elmeguid, Phys. Rev. Lett. **98**, 176406 (2007).

[5] J. S. Zhou, L. G. Marshall, and J. B. Goodenough, Phys. Rev. B - Condens. Matter Mater. Phys. **89**, 1 (2014).

[6] H. Park, A. J. Millis, and C. A. Marianetti, Phys. Rev. Lett. **109**, 1 (2012).

[7] S. Johnston, A. Mukherjee, I. Elfimov, M. Berciu, and G. A. Sawatzky, Phys. Rev. Lett. **112**, 106404 (2014).

[8] V. Bisogni, S. Catalano, R. J. Green, M. Gibert, R. Scherwitzl, Y. Huang, V. N. Strocov, P. Zubko, S. Balandeh, J. Triscone, G. Sawatzky, and T. Schmitt, Nat. Commun. **7**, 13017 (2016).

[9] T. Mizokawa, D. I. Khomskii, and G. A. Sawatzky, Phys. Rev. B **61**, 4 (1999).

[10] J. Varignon, M. N. Grisolia, J. Íñiguez, A. Barthélémy, and M. Bibes, Npj Quantum Mater. 21 (2016).

[11] A. Subedi, arXiv:1708.08899 (2017).

[12] J. Shamblin, M. Heres, H. Zhou, J. Sangoro, M. Lang, J. Neuefeind, J. A. Alonso, and S. Johnston, Nat. Commun. **9**, 86 (2018).

[13] B. Li, D. Louca, S. Yano, L. G. Marshall, J. Zhou, and J. B. Goodenough, Adv. Electron. Mater. **2**, 1 (2016).

[14] H. Guo, Z. W. Li, L. Zhao, Z. Hu, C. F. Chang, C.-Y. Kuo, W. Schmidt, A. Piovano, T. W. Pi, O. Sobolev, D. I. Khomskii, L. H. Tjeng, and A. C. Komarek, Nat. Commun. **In press**, DOI: 10.1038/s41467 (2018).

[15] A. S. Disa, F. J. Walker, S. Ismail-Beigi, and C. H. Ahn, APL Mater. **3**, 62303 (2015).

[16] M. Medarde, M. T. Fernández-Díaz, and P. Lacorre, Phys. Rev. B **78**, 212101 (2008).

[17] S. J. Allen, A. J. Hauser, E. Mikheev, J. Y. Zhang, N. E. Moreno, J. Son, D. G. Ouellette, J. Kally, A. Kozhanov, L. Balents, and S. Stemmer, APL Mater. **3**, (2015).

[18] S. Lee, R. Chen, and L. Balents, Phys. Rev. B - Condens. Matter Mater. Phys. **84**, 1 (2011).

[19] R. J. Green, M. W. Haverkort, and G. A. Sawatzky, Phys. Rev. B **94**, 1 (2016).

[20] D. J. Bergman, Phys. Rev. B **14**, 4304 (1976).

[21] J. L. García-Muñoz, J. Rodríguez-Carvajal, and P. Lacorre, Europhys. Lett. **20**, 241 (1992).

[22] J. Rodríguez-Carvajal, S. Rosenkranz, M. Medarde, P. Lacorre, M. Fernandez-Díaz, F. Fauth, and V. Trounov, Phys. Rev. B **57**, 456 (1998).

[23] K. Sreedhar, J. M. Honig, M. Darwin, M. McElfresh, P. M. Shand, J. Xu, B. C. Crooker, and J. Spalek, Phys. Rev. B **46**, 6382 (1992).

[24] N. Y. Vasanthacharya, P. Ganguly, J. B. Goodenough, and C. N. R. Rao, J. Phys. C Solid State Phys. **17**, 2745 (1984).

[25] J. B. Goodenough and P. M. Raccah, J. Appl. Phys. **36**, 1031 (1965).

[26] W. C. C. Koehler and E. O. O. Wollan, J. Phys. Chem. Solids **2**, 100 (1957).

[27] J. A. Alonso, M. J. Martínez-Lope, M. T. Casais, J. L. García-Muñoz, and M. T. Fernandez-Diaz, Phys. Rev. B. **61**, 1756 (2000).

[28] U. Staub, G. I. Meijer, F. Fauth, R. Allenspach, J. G. Bednorz, J. Karpinski, S. M. Kazakov, L. Paolasini, and F. D'Acapito, Phys. Rev. Lett. **88**, 126402 (2002).

[29] J. Zhang, H. Zheng, Y. Ren, and J. F. Mitchell, Cryst. Growth Des. **17**, 2730 (2017).

[30] Y. Kumar, A. P. Singh, S. K. Sharma, R. J. Choudhary, P. Thakur, M. Knobel, N. B. Brookes, and R. Kumar, Thin Solid Films **619**, 144 (2016).

[31] K. Tsubouchi, I. Ohkubo, H. Kumigashira, Y. Matsumoto, T. Ohnishi, M. Lippmaa, H. Koinuma, and M. Oshima, Appl. Phys. Lett. **92**, 1 (2008).

[32] J. Son, J. M. Lebeau, S. J. Allen, and S. Stemmer, Appl. Phys. Lett. **97**, 202109 (2010).

[33] J. Son, P. Moetakef, J. M. Lebeau, D. Ouellette, L. Balents, S. J. Allen, and S. Stemmer, Appl. Phys. Lett. **96**, 62114 (2010).

[34] M. Gibert, P. Zubko, R. Scherwitzl, J. Íñiguez, and J. M. Triscone, Nat. Mater. **11**, 195 (2012).

[35] M. Gibert, M. Viret, A. Torres-Pardo, C. Piamonteze, P. Zubko, N. Jaouen, J. M. Tonnerre, A. Mougin, J. Fowlie, S. Catalano, A. Gloter, O. Stéphan, and J. M. Triscone, Nano Lett. **15**, 7355 (2015).

[36] J. Hoffman, I. C. Tung, B. B. Nelson-Cheeseman, M. Liu, J. W. Freeland, and A. Bhattacharya, Phys. Rev. B **88**, 144411 (2013).

[37] T. Moriga, O. Usaka, T. Imamura, I. Nakabayashi, I. Matsubara, T. Kinouchi, S. Kikkawa, and F. Kanamaru, Bull. Chem. Soc. Jpn. **67**, 687 (1994).

[38] T. Moriga, O. Usaka, I. Nakabayashi, Y. Hirashima, T. Kohno, S. Kikkawa, and F. Kanamaru, Solid State Ionics **74**, 211 (1994).

[39] S. Rosenkranz and R. Osborn, Pramana - J. Phys. **71**, 705 (2008).

[40] J. M. González-Calbet, M. J. Sayagués, and M. Vallet-Regi, Solid State Ionics **33**, 721 (1989).

[41] See Supplemental Material at [URL will be inserted by publisher] to view the supplementary figures.

[42] T. Moriga, O. Usaka, I. Nakabayashi, T. Kinouchi, S. Kikkawa, and F. Kanamaru, Solid State Ionics **79**, 252 (1995).

[43] R. Sanchez, M. Causa, A. Caneiro, A. Butera, M. Vallet-Regi, M. Sayagues, J. Gonzalez-Calbet, F. Garcia-Sanz, and J. Rivas, Phys. Rev. B **54**, 574 (1996).

[44] J. A. Alonso, M. J. Martínez-Lope, J. L. García-Muñoz, and M. T. Fernández, Phys. B **234**–**236**, 18 (1997).

[45] K. Vidyasagar, A. Reller, J. Gopalakrishnan, and C. N. R. Rao, J. Chem. Soc. Chem. Commun. **0**, 7 (1985).

[46] J. A. Alonso, M. J. Martínez-Lope, J. L. García-Muñoz, and M. T. Fernández-Díaz, J. Phys, Condens. Matter **9**, 6417 (1997).

[47] C. N. R. Rao, J. Gopalakrishnan, K. Vidyasagar, A. K. Ganguli, A. Ramanan, and L. Ganapathi, J. Mater. Res. **1**, 280 (1986).

[48] A. M. Glazer, Acta Crystallogr. Sect. B Struct. Crystallogr. Cryst. Chem. **28**, 3384 (1972).